Spectrochimica Acta Part A: Molecular and Biomolecular Spectroscopy 108 (2013) 100–114

Contents lists available at SciVerse ScienceDirect

Spectrochimica Acta Part A: Molecular and Biomolecular Spectroscopy

journal homepage: www.elsevier.com/locate/saa

Conformational, structural, vibrational and quantum chemical analysis on 4-aminobenzohydrazide and 4-hydroxybenzohydrazide – A comparative study

V. Arjunan [a,*], A. Jayaprakash [b], K. Carthigayan [c], S. Periandy [d], S. Mohan [e]

[a] *Department of Chemistry, Kanchi Mamunivar Centre for Post-Graduate Studies, Puducherry 605 008, India*
[b] *Department of Physics, Rajiv Gandhi College of Engineering and Technology, Puducherry 605 402, India*
[c] *Research and Development Centre, Bharathiar University, Coimbatore 641 046, India*
[d] *Department of Physics, Tagore Arts College, Puducherry 605 008, India*
[e] *Department of Physics, Hawassa University Main Campus, Hawassa, Ethiopia*

H I G H L I G H T S

- ▶ The vibrational analysis of 4-hydroxybenzohydrazide and 4-aminobenzohydrazide were performed.
- ▶ The experimental parameters were compared with DFT–B3LYP calculations.
- ▶ The effect of —NH_2 and —OH in the benzohydrazide moiety have been analysed.
- ▶ Kinetic and thermodynamic stabilities and chemical hardness of the molecules were determined.
- ▶ The reactive centres were found from the electrostatic potential of the molecules.

G R A P H I C A L   A B S T R A C T

The complete vibrational analyses of the fundamental modes of 4-hydroxybenzohydrazide (4HBH) and 4-aminobenzohydrazide (4ABH) molecules were performed. The experimental parameters were compared with the theoretical parameters of the compounds determined from the DFT–B3LYP gradient calculations employing the 6-31G**, 6-311++G** and aug-cc-pVDZ basis sets. The effect of substituents —NH_2 and —OH in the benzohydrazide moiety have been analysed and compared. The kinetic and thermodynamic stability and chemical hardness of the molecules have been determined. The reactive centres were found from the molecular electrostatic potential of the molecules.

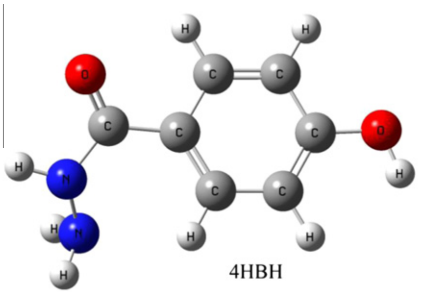

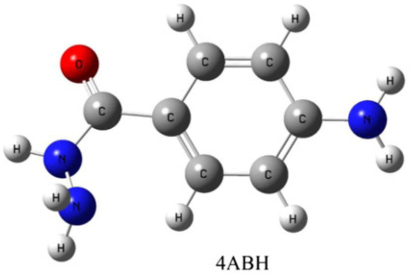

A R T I C L E   I N F O

Article history:
Received 8 December 2012
Received in revised form 29 January 2013
Accepted 31 January 2013
Available online 9 February 2013

Keywords:
4-Hydroxybenzohydrazide
4-Aminobenzohydrazide
FTIR
FT-Raman
NBO
MEP

A B S T R A C T

Experimental and theoretical quantum chemical studies were carried out on 4-hydroxybenzohydrazide (4HBH) and 4-aminobenzohydrazide (4ABH) using FTIR and FT-Raman spectral data. The structural characteristics and vibrational spectroscopic analysis were carried performed by quantum chemical methods with the hybrid exchange-correlation functional B3LYP using 6-31G**, 6-311++G** and aug-cc-pVDZ basis sets. The most stable conformer of the title compounds have been determined from the analysis of potential energy surface. The stable molecular geometries, electronic and thermodynamic parameters, IR intensities, harmonic vibrational frequencies, depolarisation ratio and Raman intensities have been computed. Molecular electrostatic potential and frontier molecular orbitals were constructed to understand the electronic properties. The potential energy distributions (PEDs) were calculated to explain the mixing of fundamental modes. The theoretical geometrical parameters and the fundamental frequencies were compared with the experimental. The interactions of hydroxy and amino group substitutions on the characteristic vibrations of the ring and hydrazide group have been analysed.

---

* Corresponding author. Tel.: +91 413 2211111, mobile: +91 9442992223; fax: +91 413 2251613.
E-mail address: varjunftir@yahoo.com (V. Arjunan).

1386-1425/$ - see front matter © 2013 Elsevier B.V. All rights reserved.
http://dx.doi.org/10.1016/j.saa.2013.01.076

Introduction

High temperature resistive polymers have been the subject of considerable investigation in recent years owing to their ability to exhibit high thermo-oxidative stability, resistance to environmental degradation, and superior dielectric, thermal, adhesive, dimensional stability and mechanical properties [1–7]. These properties are strongly influenced by their chemical structure, i.e. by both the chemical composition and molecular configuration. In particular, polymers containing aromatic rings in the main chain have received special attention as their presence makes these polymers more thermally resistant [8–10]. In this connection, the introduction of hydrazide or amide plus hydrazide linkages into the backbone of the polymer chain is a viable alternative to improve the processability of high temperature resistive polymers. Further, the presence of hydrazide groups in the main chain can be exploited by converting them into the more chemically resistant and thermally stable oxadiazole structure by heating the polymer in the bulk or fibre form at elevated temperatures [11]. Hydrazides are known to have different biological activities [12–14].

Hydrazides are important starting materials for a wide range of derivatives utilizable in pharmaceutical products and as surfactants [15]. Hydrazides have been known to be associated with antibacterial [16], antifungal [17], anthelmintic [18] and anticonvulsant [19] activities. Biological assessment of fatty hydrazide and their derivatives have been studied [20,21]. Acylhydrazones, as an example of Schiff bases, and their metal complexes have been widely studied due to their versatile applications in the fields of analytical and medicinal chemistry and biotechnology [22–24]. *p*-Hydroxy benzohydrazide moiety and its analogues are suitable parent compounds upon which variety of biological activities were reported such as antitumor [25], antianginal [26], antitubercular [27], antihypertensive [28] and antibacterial [29].

Generally the donor–acceptor substituted π-conjugated organic molecules (e.g. nitroaniline) only exhibit large molecular nonlinear optical (NLO) response. But there no experimental evidence of NLO properties of benzohydrazide and its derivatives as such in the literature. NLO properties are not possible for the compounds under investigation since they contain only donar groups. At the same time benzohydrazide and its derivatives act as donar (ligand) in the complexes which exhibits NLO properties [30,31]. The nonlinear response in these molecules was found to increase with increase in the donor strength of the substituted group.

Hydrazides have recently become attractive to theoreticians as well as experimentalists due to the biological significance particularly in medicinal and enzyme chemistry [32–37]. In continuation of our earlier studies [38] and owing to the vast biological significance and industrial applications of 4-aminobenzohydrazide (4ABH) and 4-hydroxybenzohydrazide (4HBH) in an enormous field, an extensive spectroscopic and structural study of these compounds have been undertaken by recording their FTIR and FT-Raman spectra and subjecting them to DFT analysis. The effects of hydroxyl and amino groups on the characteristic frequencies of the benzene ring moiety and hydrazide groups have been analysed.

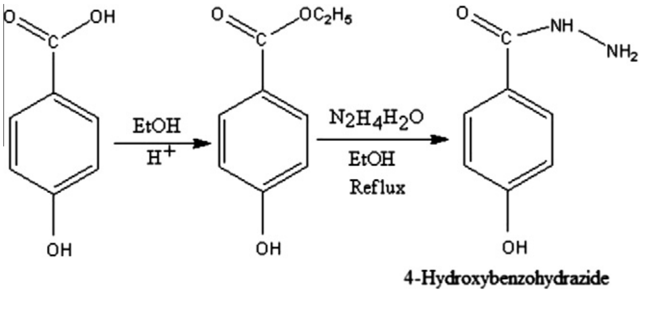

Scheme 1. Synthesis of 4-hydroxybenzohydrazide.

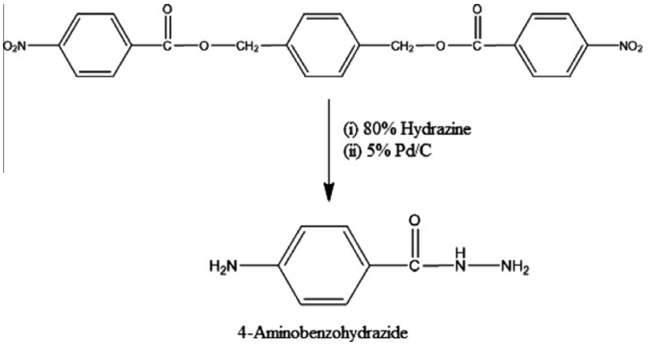

Scheme 2. Synthesis of 4-aminobenzohydrazide.

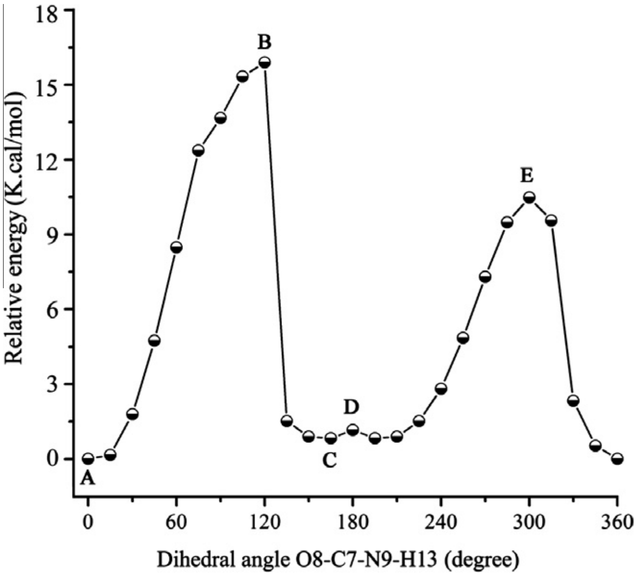

Fig. 1. Potential energy surface of 4-hydroxybenzohydrazide.

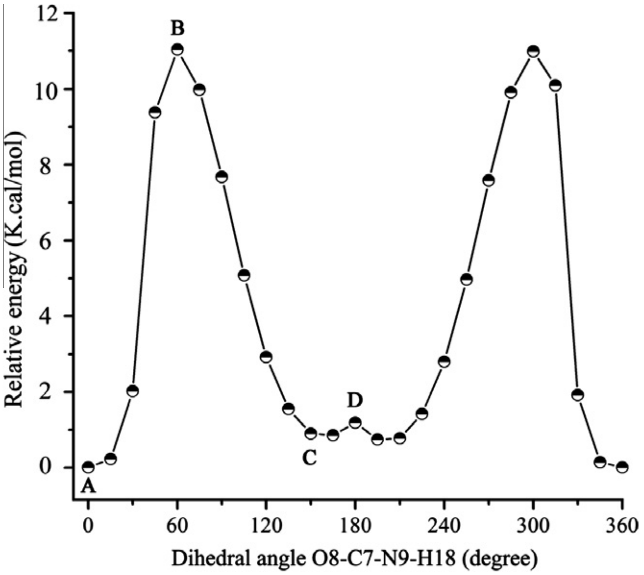

Fig. 2. Potential energy surface of 4-aminobenzohydrazide.

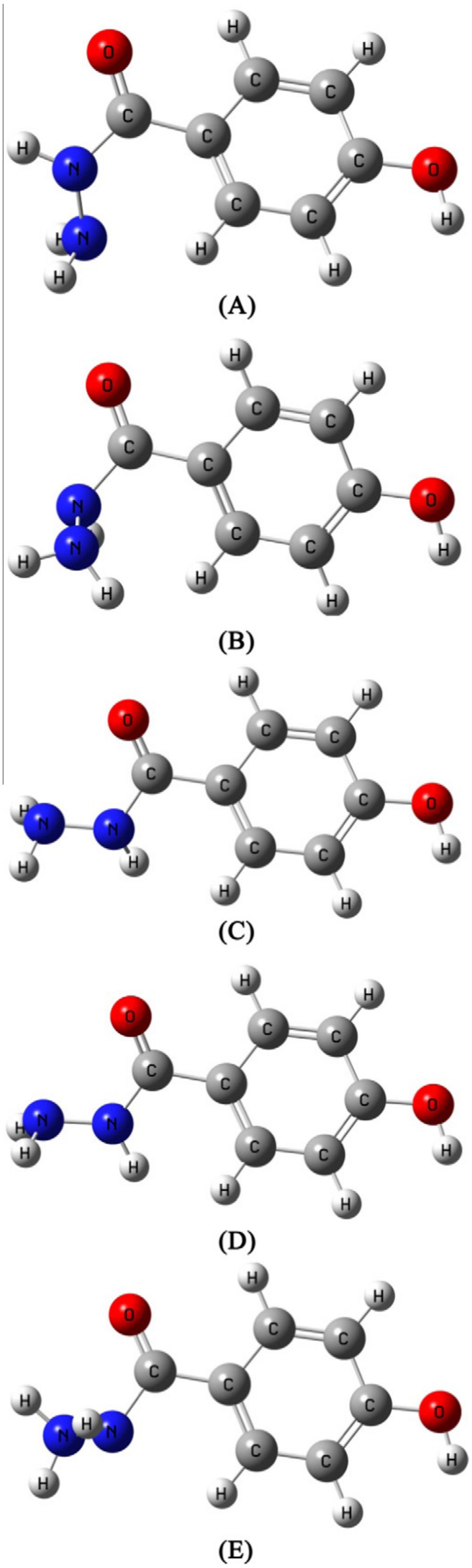

Fig. 3. Possible conformers of 4-hydroxybenzohydrazide.

Thus, the novelty of the investigation is to provide more detailed structural, conformational, vibrational, energies, stabilities and thermodynamic properties of 4ABH and 4HBH.

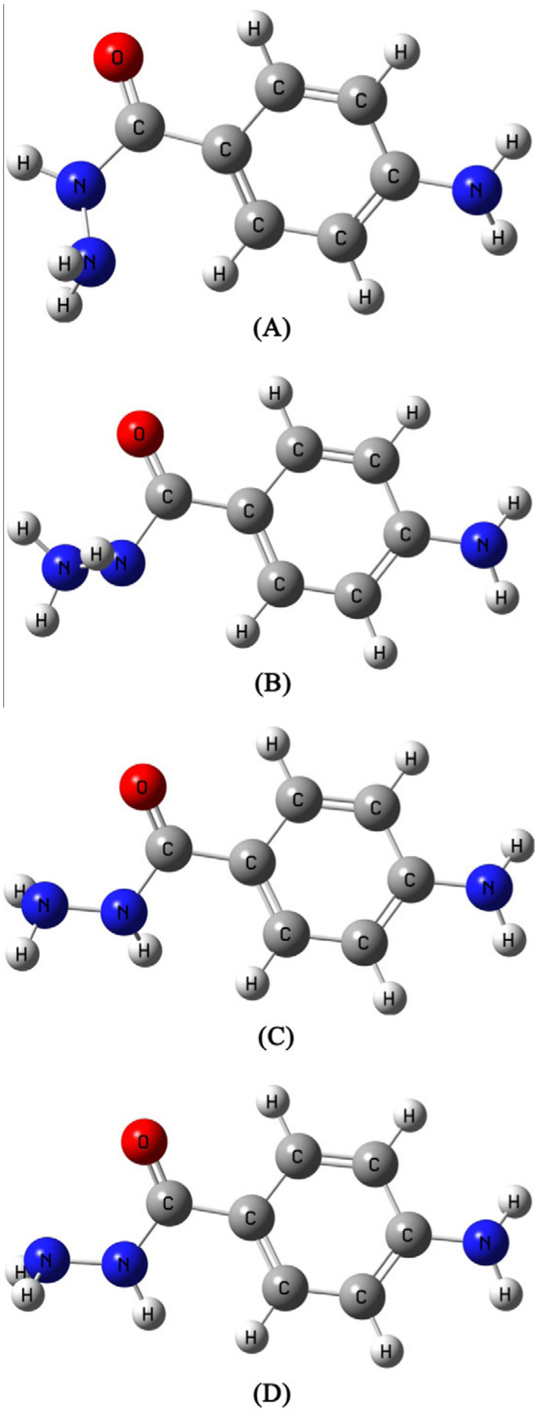

Fig. 4. Various conformers of 4-aminobenzohydrazide.

Experimental

4-Hydroxybenzohydrazide (4HBH) was synthesised from the corresponding acid through a conventional two step approach (Scheme 1). All chemicals were obtained from Aldrich, U.S.A. and were used without further purification. 3.45 g of hydroxybenzoic acid is dissolved in 75 ml of dry ethanol and 2–3 drops of con. H_2SO_4 are added, the mixture was stirred well for 2 h. The ester 4-hydroxyethylbenzoate was extracted with chloroform solvent and evaporated by rotary evaporator. Then refluxing 4-hydroxyethylbenzoate (0.1 mol) with hydrazine hydrate (0.15 mol) in

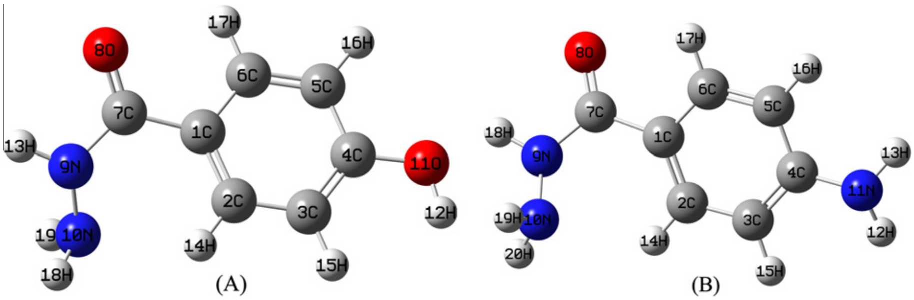

Fig. 5. Structure and atom numbering of 4-hydroxybenzohydrazide (A) and 4-aminobenzohydrazide (B).

Table 1
Theoretical and experimental structural parameters of 4-aminobenzohydrazide and 4-hydroxybenzohydrazide.

Structural parameters	4-Aminobenzohydrazide			Structural parameters	4-Hydroxybenzohydrazide			Experimental parameters[a]
	B3LYP/6-31G**	B3LYP/6-311++G**	B3LYP/aug-cc-pVDZ		B3LYP/6-31G**	B3LYP/6-311++G**	B3LYP/aug-cc-pVDZ	
Internuclear distance (Å)								
C1—C2	1.403	1.401	1.405	C1—C2	1.406	1.403	1.409	1.385
C2—C3	1.390	1.389	1.393	C2—C3	1.387	1.386	1.389	1.386
C3—C4	1.407	1.404	1.408	C3—C4	1.400	1.397	1.403	1.377
C4—C5	1.408	1.406	1.409	C4—C5	1.399	1.397	1.401	1.379
C5—C6	1.387	1.385	1.390	C5—C6	1.392	1.391	1.395	1.378
C6—C1	1.403	1.401	1.405	C6—C1	1.402	1.399	1.405	1.380
C1—C7	1.499	1.499	1.499	C1—C7	1.494	1.494	1.500	1.473
C7—O8	1.221	1.216	1.222	C7—O8	1.229	1.224	1.229	1.229
C7—N9	1.389	1.386	1.388	C7—N9	1.387	1.386	1.387	1.365
N9—N10	1.402	1.399	1.403	N9—N10	1.406	1.406	1.403	1.372
C—H (ring)[b]	1.086	1.084	1.090	C—H (ring)[b]	1.084	1.083	1.090	0.930
N—H (hydrazide)[b]	1.014	1.011	1.014	N—H (hydrazide)[b]	1.017	1.015	1.021	0.860
N—H (amino)[b]	1.010	1.008	1.011	C4—O11	1.364	1.366	1.362	1.357[c]
C4—N11	1.389	1.389	1.392	O11—H12	0.966	0.963	0.969	0.80[c]
Bond angle (°)								
C2—C1—C6	118.1	118.0	118.0	C2—C1—C6	118.4	118.5	118.1	121.1
C2—C1—C7	124.3	124.2	124.1	C2—C1—C7	125.6	124.9	126.5	119.5
C6—C1—C7	117.6	117.7	117.8	C6—C1—C7	115.9	116.5	115.3	119.5
C1—C2—C3	121.1	121.2	121.2	C1—C2—C3	120.6	120.6	120.7	120.5
C2—C3—C4	120.5	120.5	120.5	C2—C3—C4	120.2	120.1	120.4	119.2
C3—C4—C5	118.4	118.4	118.5	C3—C4—C5	119.4	119.1	119.6	119.8
C4—C5—C6	120.6	120.6	120.6	C4—C5—C6	120.0	120.2	119.7	119.8
C1—C6—C5	121.3	121.2	121.3	C1—C6—C5	121.4	121.3	121.6	118.1
C1—C2—H14	120.2	120.4	120.5	C1—C2—H14	119.9	120.0	119.6	120.0
C3—C2—H14	118.6	118.4	118.3	C3—C2—H14	119.5	119.5	119.6	121.1
C2—C3—H15	120.0	119.9	119.9	C2—C3—H15	119.9	119.9	119.8	119.9
C4—C3—H15	119.5	119.6	119.6	C4—C3—H15	119.9	120.0	119.8	119.9
C3—C4—N11	120.8	120.8	120.7	C3—C4—O11	122.6	122.6	122.8	1195
C5—C4—N11	120.7	120.7	120.7	C5—C4— O11	117.5	117.5	117.6	119.5
C4—C5—H16	119.4	119.5	119.6	C4—C5—H16	119.0	119.1	118.9	119.5
C6—C5—H16	120.0	119.9	119.9	C6—C5—H16	121.5	121.3	121.5	119.5
C1—C6—H17	118.1	118.3	118.3	C1—C6— H17	118.0	118.4	117.8	118.5
C5—C6—H17	120.7	120.4	120.4	C5—C6— H17	120.5	120.2	120.6	123.4
C1—C7—O8	122.4	122.4	122.3	C1—C7—O8	121.4	121.4	121.0	121.7
C1—C7—N9	114.2	114.2	114.6	C1—C7—N9	121.1	120.6	121.9	115.7
O8—C7—N9	123.4	123.3	123.1	O8—C7—N9	117.5	118.0	117.7	122.5
C7—N9—N10	119.0	119.9	119.4	C7—N9—N10	123.9	124.0	124.8	121.0
C7—N9—H18	116.2	117.4	116.9	C7—N9—H13	110.5	111.6	110.7	121.0
N10—N9—H18	118.6	118.7	118.4	N10—N9—H13	118.8	118.6	119.2	118.1
N9—N10—H19	111.1	111.9	111.5	N9—N10—H18	108.9	109.5	108.8	
N9—N10—H20	108.9	110.1	109.4	N9—N10—H19	110.6	111.0	110.4	
H19—N10—H20	109.2	110.6	109.7	H18—N10—H19	108.4	109.3	107.3	
C4— N—H (amino)[b]	116.2	116.9	116.7	C4—O11—H12	109.1	109.8	108.8	109.5[c]
H12—N11—H13	112.8	113.3	113.2					

[a] Values taken from Ref. [48].
[b] Mean value.
[c] Values taken from Ref. [39].

75 ml of dry ethanol for 5–6 h to form benzohydrazide. The product was filtered, washed with hexene and dried. The product was recrytallised with methanol and dried in air. The melting point of 4-hydroxybenzohydrazide is 265 °C. All elemental analysis (C, H,

Table 2
The thermodynamic parameters of 4-aminobenzohydrazide and 4-hydroxybenzohydrazide.

Thermodynamic parameters (298 K)	4-Aminobenzohydrazide B3LYP			4-Hydroxybenzohydrazide B3LYP		
	6-31G**	6-311++G**	aug-cc-pVDZ	6-31G**	6-311++G**	aug-cc-pVDZ
Total energy (thermal), E_{total} (kcal mol^{-1})	107.69	107.19	107.03	99.91	99.41	99.52
Heat capacity at const. volume, C_v (kcal mol^{-1} K^{-1})	39.66	40.00	40.08	37.75	38.06	37.70
Entropy, S (kcal mol^{-1} K^{-1})	99.35	100.02	100.23	97.94	98.27	98.68
Vibrational energy, E_{vib} (kcal mol^{-1})	105.92	105.42	105.25	98.13	97.63	97.75
SCF (Hartrees)	−511.6349	−511.7750	−511.6993	−531.4991	−531.6463	−531.5224
Rotational constants (GHz)						
X	3.35	3.36	3.35	2.51	2.51	2.52
Y	0.56	0.56	0.56	0.66	0.66	0.66
Z	0.49	0.49	0.49	0.54	0.54	0.53
Dipolemoment (Debye)						
μ_x	−2.90	−3.01	−3.01	0.84	0.69	0.92
μ_y	−4.33	−4.42	−4.29	−4.69	−4.89	−4.75
μ_z	3.19	2.91	2.84	1.00	0.89	0.61
μ_{total}	6.11	6.09	5.96	4.86	5.02	4.87

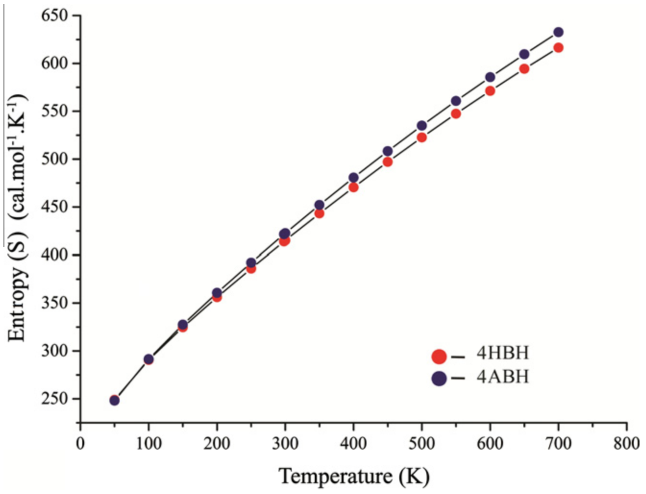

Fig. 6. Temperature dependence of entropy of 4-hydroxybenzohydrazide (4HBH) and 4-aminobenzohydrazide (4ABH).

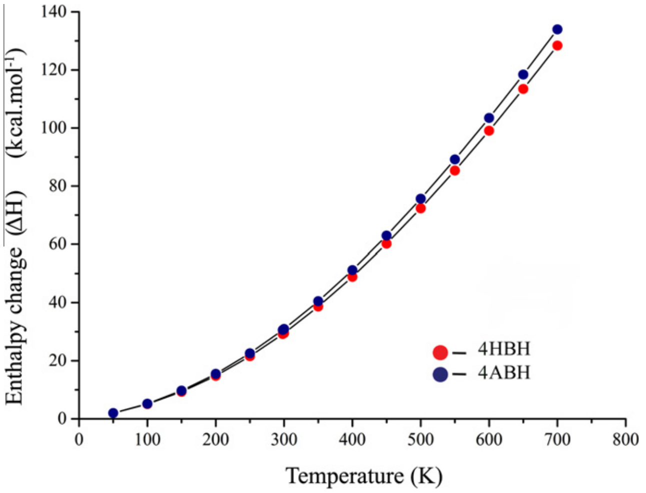

Fig. 8. Temperature dependence of enthalpy change of 4-hydroxybenzohydrazide (4HBH) and 4-aminobenzohydrazide (4ABH).

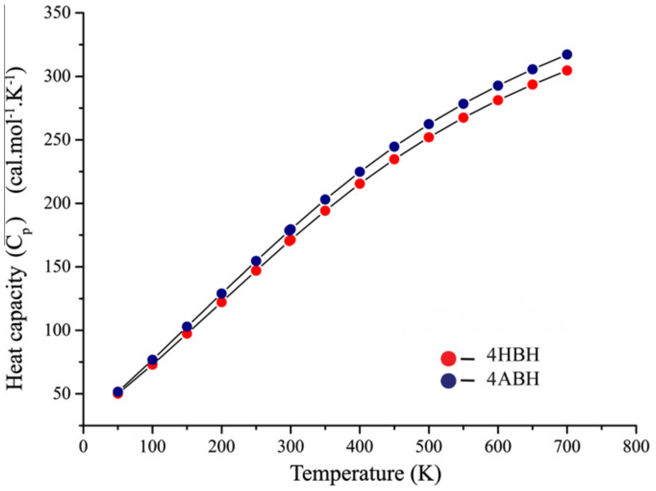

Fig. 7. Temperature dependence of heat capacity at constant pressure of 4-hydroxybenzohydrazide (4HBH) and 4-aminobenzohydrazide (4ABH).

N) were carried out on a Perkin Elmer 2400 CHN elemental analyser. The calculated (found)% for $C_7H_8N_2O_2$: C, 54.55 (53.85); H, 5.26 (5.11) and N, 18.42 (18.10).

Table 3
The energy of frontier molecular orbitals of 4-aminobenzohydrazide and 4-hydroxybenzohydrazide determined by DFT methods.

Energy level	4-Aminobenzohydrazide B3LYP		4-Hydroxybenzohydrazide B3LYP	
	6-311++G**	aug-cc-pVDZ	6-311++G**	aug-cc-pVDZ
E_{LUMO} (a.u.)	−0.0341	−0.0355	−0.0409	−0.0261
E_{HOMO} (a.u.)	−0.2216	−0.2211	−0.2378	−0.2254
$E_g = E_{LUMO} - E_{HOMO}$ (a.u.)	0.1875	0.1856	0.1969	0.1993
E_{LUMO+1} (a.u.)	−0.0231	−0.0240	−0.0241	−0.0054
E_{HOMO-1} (a.u.)	−0.2517	−0.2495	−0.2604	−0.2449
$E_g = E_{LUMO-1} - E_{HOMO+1}$ (a.u.)	0.2286	0.2255	0.2363	0.2395

4-Aminobenzohydrazide (4ABH) was synthesised using the reported procedure [39] by Scheme 2. 1.0 g of 1,4-bis(4-nitrobenzoyloxymethyl)benzene and 10 ml of hydrazine monohydrate were added in 80 ml of ethanol and refluxed for an hour. Then 0.2 g of 5% palladium on carbon (Pd/C) was added and further refluxed for 15 h and filtered hot to remove Pd/C. Then it is allowed to cool and the crude solid was recrystallised from ethanol and dried in air to afford 4-aminobenzohydrazide. The melting point

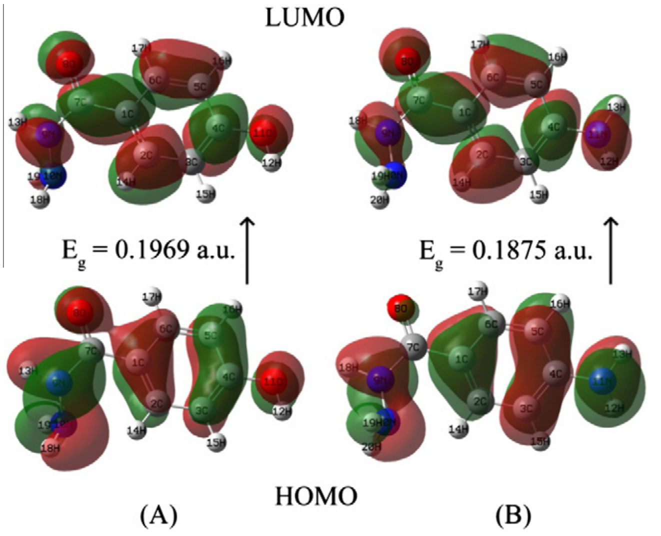

Fig. 9. Frontier molecular orbital of 4-hydroxybenzohydrazide (A) and 4-aminobenzohydrazide (B).

Table 4
Atomic charges of 4-hydroxybenzohydrazide and 4-aminobenzohydrazide calculated by NBO at B3LYP/6-311++G** level.

Atom	4-Hydroxybenzohydrazide	4-Aminobenzohydrazide
C1	−0.1747	−0.1781
C2	−0.1373	−0.1360
C3	−0.2907	−0.2633
C4	0.3345	0.1871
C5	−0.2557	−0.2562
C6	−0.1339	−0.1302
C7	0.6682	0.6545
O8	−0.6265	−0.5986
N9	−0.4781	−0.5076
N10	−0.6398	−0.6283
O11	−0.6669	
N11		−0.7813
H12	0.4672	0.3745
H13	0.3682	0.3753
H14	0.2181	0.2019
H15	0.2005	0.1977
H16	0.2198	0.2007
H17	0.2286	0.2318
H18	0.3503	0.3602
H19	0.3483	0.3545
H20		0.3414

of 4-aminobenzohydrazide is 226 °C. All elemental analysis (C, H, N) were carried out on a Perkin Elmer 2400 CHN elemental analyser. The calculated (found)% for $C_7H_8N_2O_2$: C, 55.63 (55.25); H, 5.96 (5.92) and N, 27.81 (27.75).

The FTIR spectra of 4ABH and 4HBH have been recorded in the region between 4000 and 400 cm^{-1} by KBr disc method using Bruker IFS 66 V spectrometer. A KBr beam splitter and liquid nitrogen cooled MCT detector were used to collect the mid-infrared spectra. The FT-Raman spectra were also recorded in the range between 4000 and 100 cm^{-1} by the same instrument with FRA 106 Raman module equipped with Nd:YAG laser source with 200 mW power operating at 1.064 μm. The spectral resolution is 2 cm^{-1}.

Computational details

The gradient corrected density functional theory (DFT) with the three-parameter hybrid functional Becke3 (B3) [40,41] for the exchange part and the Lee–Yang–Parr (LYP) correlation functional [42] level of calculations have been carried out in the present

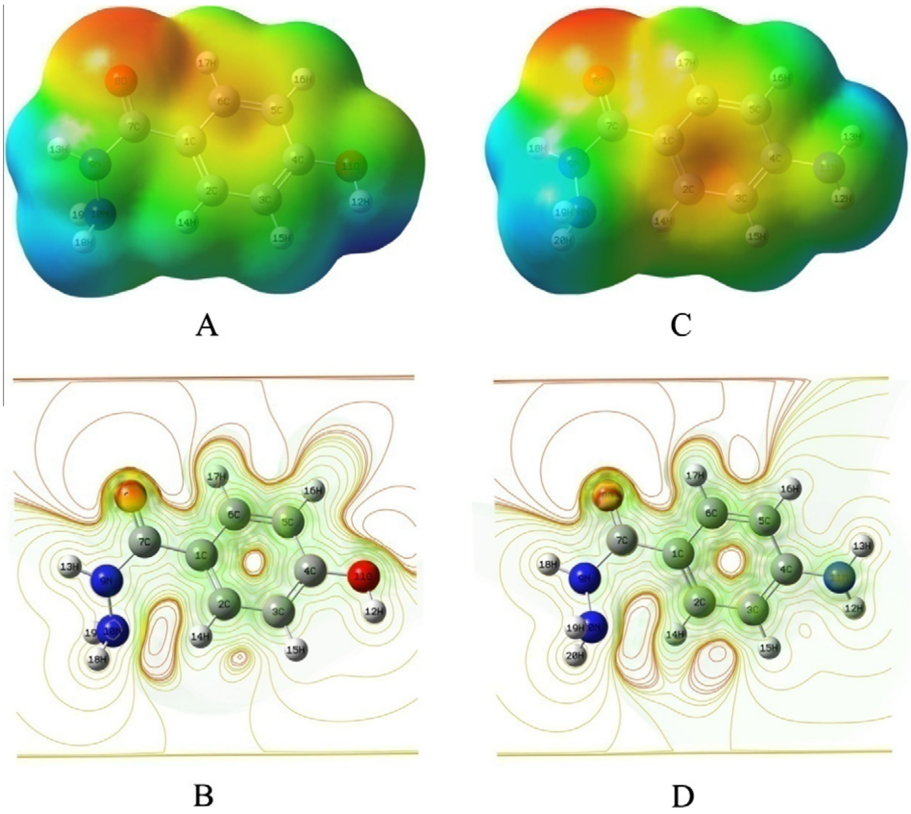

Fig. 10. MESP and electrostatic potential contour maps of 4-hydroxybenzohydrazide (A and B) and 4-aminobenzohydrazide (C and D).

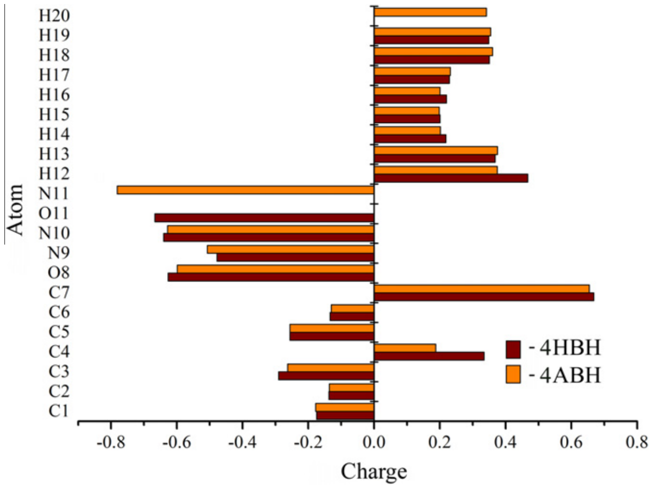

Fig. 11. Atomic charges correlation graph between 4-hydroxybenzohydrazide and 4-aminobenzohydrazide.

investigation, using 6-31G**, 6-311++G** and aug-cc-pVDZ basic sets with Gaussian-03W [43] program.

The conformational analyses were performed and the energies of the different possible conformers were found. The geometry of the different conformers of the compounds were optimised with B3LYP method using 6-31G**, 6-311++G** and aug-cc-pVDZ basis sets to characterise all stationary points as minima. The optimised structural parameters of the most stable conformer were used in the vibrational frequency calculations. The potential energy distributions corresponding to each of the observed frequencies were calculated with the program of Fuhrer et al. [44].

Isoelectronic molecular electrostatic potential have been calculated using 6-311++G** basis set. The molecular electrostatic potential (MEP) at a point r in the space around a molecule (in atomic units) can be expressed as:

$$V(r) = \sum_A \frac{Z_A}{|\vec{R}_A - \vec{r}|} - \int \frac{\rho(\vec{r}')d\vec{r}'}{|\vec{r}' - \vec{r}|}$$

where Z_A is the charge on nucleus A, located at R_A and $\rho(r')$ is the electronic density function for the molecule. The first and second terms represent the contributions to the potential due to nuclei and electrons, respectively. $V(r)$ is the resultant at each point r, which is the net electrostatic effect produced at the point r by both the electrons and nuclei of the molecule. GaussView 5.0.8 visualisation program [45] has been utilised to construct the optimised molecular structures, MEP surface and the shape of HOMO and LUMO orbitals.

The Raman scattering activities (S_i) calculated by Gaussian 03W program were suitably converted to relative Raman intensities (I_i) using the following relationship derived from the basic theory of Raman scattering [46].

$$I_i = \frac{f(\nu_0 - \nu_i)^4 S_i}{\nu_i[1 - \exp(-hc\nu_i/kT)]}$$

where ν_0 is the exciting frequency (cm^{-1}), ν_i is the vibrational wavenumber of the ith normal mode, h, c and k are universal constants, and f is the suitably chosen common scaling factor for all the peak intensities.

Results and discussion

Conformational analysis

To find all possible conformers and also the most stable geometry of 4HBH and 4ABH molecules conformation analysis was carried out by using B3LYP/6-311++G** method. During the potential energy surface scan, all the geometrical parameters were simultaneously relaxed while the dihedral angle O8—C7—N9—H13 of 4HBH and O8—C7—N9—H18 of 4HBH are varied in steps of 15° ranging from 0° to 360°. The potential energy surface of 4HBH and 4ABH were shown in Figs. 1 and 2, respectively. The energy profile of 4HBH shows five conformers A, B, C, D and E with relative energies 0.0, 16.548, 0.856, 1.201 and 10.907 kcal mol^{-1}, respectively have been shortlisted and are shown in Fig. 3. For 4ABH molecule four conformers A, B, C and D with relative energies 0.00, 10.383, 0.695, and 1.112 kcal mol^{-1}, respectively have been shortlisted and are shown in Fig. 4. Thus, the optimised geometry (A) in Figs. 3 and 4 corresponds to global minimum energy in the PES belongs to the most stable conformer of 4HBH and 4ABH molecules. The geometrical parameters, electronic, thermodynamic properties and vibrational frequencies were determined by B3LYP method with 6-31G**, 6-311++G** and aug-cc-pVDZ basis sets.

Molecular geometry and structural properties

The energetically most stable optimised geometry of 4HBH and 4ABH obtained from B3LYP/6-311++G** method and the scheme of numbering the atoms are shown in Fig. 5. The geometry of the most stable configuration of the molecules posses C_1 point group symmetry. All vibrations are active in both IR and Raman.

Table 5
Second order perturbation theory analysis of Fock matrix by B3LYP/6-311++G** method.

Donor (i) → acceptor (j)	4-Aminobenzohydrazide			4-Hydroxybenzohydrazide		
	$E^{(2)a}$ (kJ mol^{-1})	$E(j) - E(i)^b$ (a.u.)	$F(I,j)^e$ (a.u.)	$E^{(2)a}$ (kJ mol^{-1})	$E(j) - E(i)^b$ (a.u.)	$F(I,j)^e$ (a.u.)
π(C1—C2) → π^*(C3—C4)	16.64	0.27	0.061	16.96	0.27	0.061
π(C1—C2) → π^*(C5—C6)	22.39	0.29	0.072	22.6	0.28	0.073
π(C1—C2) → π^*(C7—O8)	16.81	0.31	0.066	16.54	0.33	0.068
π(C3—C4) → π^*(C1—C2)	25.35	0.29	0.076	24.4	0.3	0.077
π(C3—C4) → π^*(C5—C6)	14.55	0.29	0.059	14.51	0.3	0.06
π(C5—C6) → π^*(C1—C2)	15.79	0.28	0.061	15.98	0.29	0.061
π(C5—C6) → π^*(C3—C4)	23.35	0.28	0.074	24.58	0.27	0.074
n(O8) → σ^*(C1—C7)	18.53	0.67	0.101	17.38	0.68	0.099
n(O8) → σ^*(C7—N9)	27.74	0.67	0.123	24.21	0.68	0.116
n(N9) → π^*(C7—O8)	37.39	0.34	0.101	32.13	0.37	0.098
n(N11) → π^*(C3—C4)	29.11	0.32	0.092			
n(O11) → π^*(C3—C4)				28.43	0.35	0.096

[a] Stabilisation (delocalization) energy.
[b] Energy difference between i(donor) and j(acceptor) NBO orbitals.
[e] Fock matrix element i and j NBO orbitals.

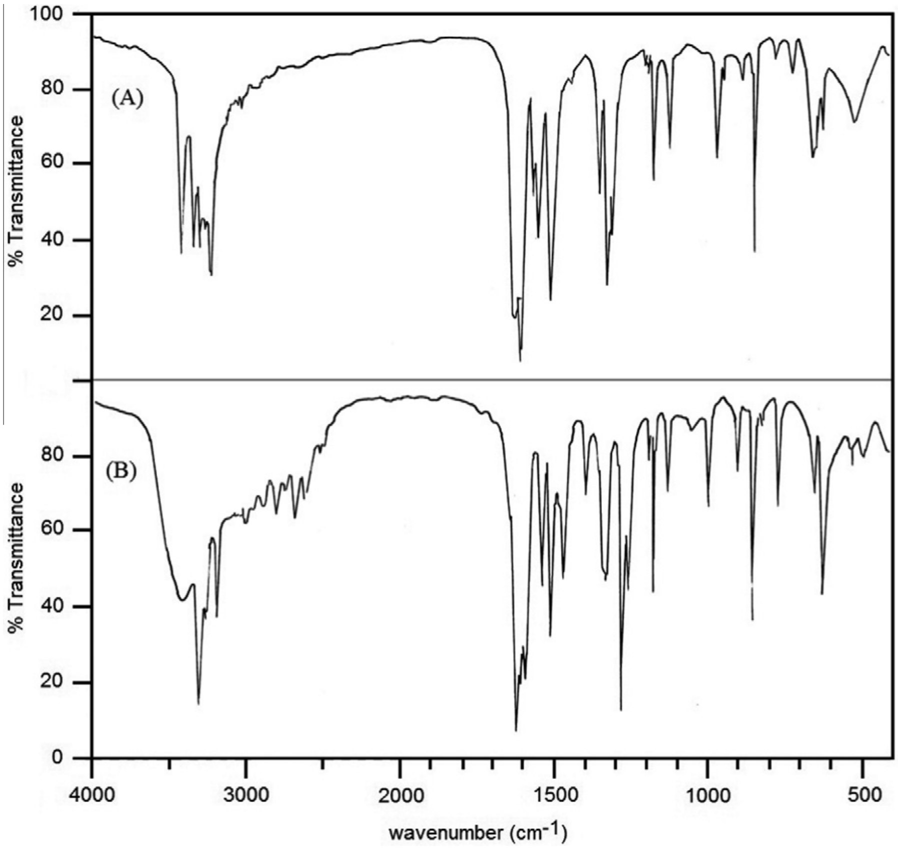

Fig. 12. FTIR spectrum of (A) 4-aminobenzohydrazide and (B) 4-hydroxybenzohydrazide.

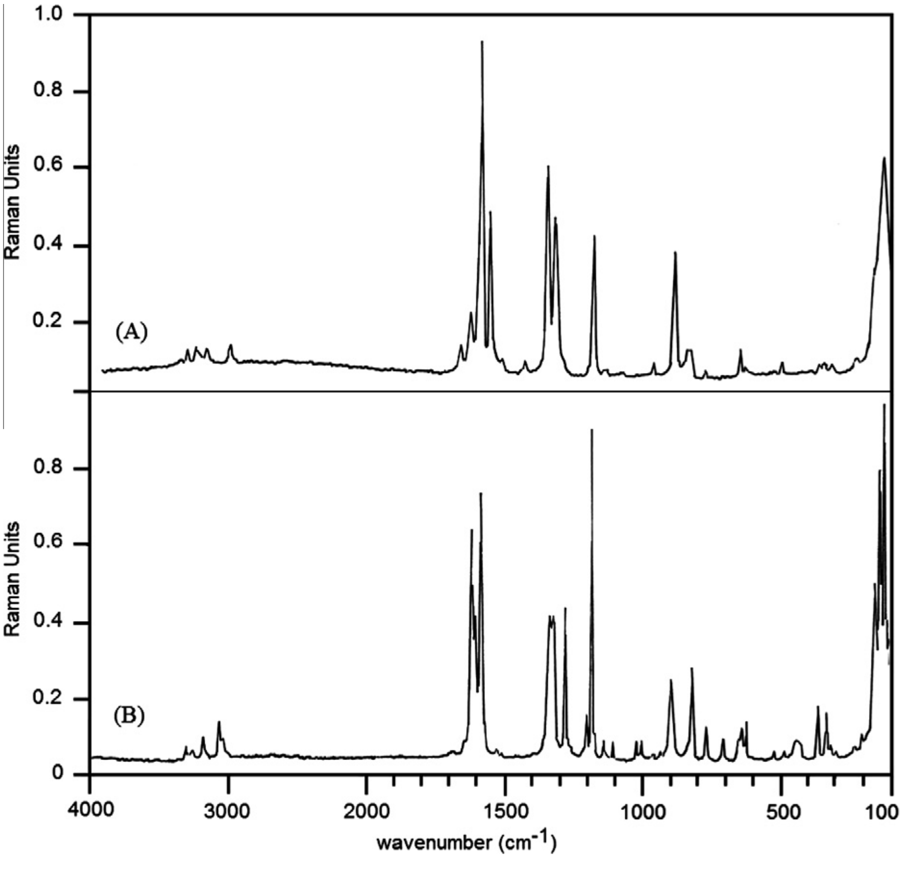

Fig. 13. FT-Raman spectrum of (A) 4-aminobenzohydrazide and (B) 4-hydroxybenzohydrazide.

The optimised structural parameters for the thermodynamically preferred geometry of 4HBH and 4ABH determined at B3LYP method using 6-31G**, 6-311++G** and aug-cc-pVDZ basis sets are presented in Table 1. The parameters derived from B3LYP/6-311++G** method were only considered for comparative discussion of the compounds due to the more reliability of this method. In 4ABH the mean planes of the benzene ring and the planar hydrazide group are inclined at 28.6° with respect to each other. But the mean planes of the benzene ring and the planar hydrazide group of 4HBH are inclined at 24.5° with respect to each other. Except amino and hydrazide hydrogens, the 4ABH and 4HBH molecules are essentially planar as evidenced by the torsion angles C6—C1—C7—O8, N10—N9—C7—C1 and N10—N9—C7—O8 of −22.6°, −178.8° and 1.0° for 4ABH while these are −23.3°, −23.2° and 158.5°, respectively for 4HBH molecule.

The aromatic C—H, N—H (hydrazide) and N—H (amino) distances of 4ABH are 1.084, 1.011 and 1.008 Å, respectively. In 4HBH the aromatic C—H, O—H and N—H distances are 1.083, 0.963 and 1.015 Å, respectively. The mean C—C bond distance of the ring carbon atoms of 4HBH and 4ABH are 1.413 and 1.412 Å, respectively. The C—H bond lengths are found to be insignificant deviation with the —OH and —NH_2 substitutions. The electron diffraction study of benzohydrazide shows the mean C—C (ring) bond distance, the C—H, C=O and C—O bond distances 1.396, 0.930, 1.229 and 1.358 Å, respectively [38]. The presence of —OH and —NH_2 substitutions leads insignificant distortion in bond lengths of the benzene ring while a slight significant distortion is absorbed in the substituent bond angles. The C—N—H bond angle where the —NH_2 group is attached with the carbon C4 is nearly 117° while the C—O—H bond angle to the substituent —OH is found to be nearly 109°.

In 4ABH, the angles about the carbonyl carbon atom (C7) ranges from 114.2 for N9—C7—C1 to 122.4 for O8—C7—C1, consistent with significant carbonyl character in the C7=O8 bond (1.216 Å). In the case of 4HBH these angles are equal to 120.6° and 121.4°, respectively. The N9—C7 bond distance of 4ABH is 1.386 Å and N9—N10 is 1.399 Å while in 4HBH these angles are 1.386° and 1.406°, respectively. These structural parameters are in good agreement with the literature [38,39,47,48].

Temperature dependence of thermodynamic properties

The frequency calculations compute the zero point energies, thermal correction to internal energy, enthalpy, Gibbs free energy and entropy as well as the heat capacity for a molecular system. The calculated thermodynamic parameters of 4HBH and 4ABH employing B3LYP method with 6-31G**, 6-311++G** and aug-cc-pVDZ basis sets are presented in Table 2.

The temperature dependence of the thermodynamic properties heat capacity at constant pressure (C_p), entropy (S) and enthalpy change ($\Delta H_{0\rightarrow T}$) for the compounds were also determined by B3LYP/6-311++G** method. The anharmonicity effects have been eliminated by scaling the thermodynamic properties by 0.98. Figs. 6–8 depicts the correlation of heat capacity at constant pressure (C_p), entropy (S) and enthalpy change ($\Delta H_{0\rightarrow T}$) with temperature. The figures reveal that the entropies, heat capacities, and enthalpy changes are increasing with temperature ranging from 50 to 700 K [49]. The observed relations of the thermodynamic functions vs. temperatures for 4HBH are

$$S = 218.46431 + 0.72186T - 2.22077 \times 10^{-4}T^2$$

$$C_p = 21816.15762 + 0.59834T - 2.61755 \times 10^{-4}T^2$$

$$\Delta H = -1.55124 + 0.04358T + 2.05264 \times 10^{-4}T^2$$

For 4ABH the corresponding relations are

$$S = 215.66442 + 0.76155T - 2.40543 \times 10^{-4}T^2$$

$$C_p = 17.09554 + 0.62815T - 2.81717 \times 10^{-4}T^2$$

$$\Delta H = -1.85155 + 0.04736T + 2.1198 \times 10^{-4}T^2$$

The regression factors (R^2) for all the relations are 0.999. Figs. 6–8 one can observe that the difference between the respective thermodynamic functions of 4HBH and 4ABH are directly proportional to the temperature.

Electronic properties

The energy of HOMO, LUMO, LUMO+1 and HOMO−1 and their orbital energy gap of 4HBH and 4ABH are calculated using B3LYP/6-311++G** method is given in Table 3. The pictorial illustrations of the frontier molecular orbitals are shown in Fig. 9. The positive and negative phase is represented in red and green[1] colour, respectively. The region of HOMO and LUMO levels spread over the entire molecule and the calculated energy gap of HOMO–LUMO's explains the ultimate charge transfer interface within the molecule. The frontier orbital energy gaps $E_g = E_{\mathrm{LUMO}} - E_{\mathrm{HOMO}}$ in case of 4HBH and 4ABH is found to be 0.1969 and 0.1875 a.u., respectively. The HOMO and LUMO reveals that there are both $\pi \rightarrow \pi^*$ and $n \rightarrow \pi^*$ charge transfer transitions in these molecules. The absolute chemical hardness has been used as a measure of kinetic stability or the reactivity of the molecule. The chemical hardness measured from the frontier molecular orbital energies of 4HBH and 4ABH is 0.09845 and 0.09375 eV, respectively. The smaller E_g and the hardness signify the high reactivity of the molecules.

The value of the electrostatic potential mapped onto an electron iso-density surface may be employed to distinguish regions on the surface which are electron rich (subject to electrophilic attack) from those which are electron deficient (subject to nucleophilic attack). The resulting surface simultaneously displays molecular size, shape and electrostatic potential in terms of colour grading and is very useful tool in investigation of correlation between molecular structure and the physiochemical property relationship of molecules including biomolecules and drugs [50,51]. The equation used to find the electrostatic potential is,

$$\text{Total electrostatic potential energy} = \sum \text{Electrostatic potential energy}$$

$$\text{Potential energy} = K\frac{q_1 q_2}{r}, \quad K = \text{Coulomb's constant}$$

MEP and electrostatic potential contour maps of 4-hydroxybenzohydrazide (A and B) and 4-aminobenzohydrazide (C and D) are depicted in Fig. 10. The colour scheme of MEP is the negative electrostatic potentials are shown in red, the intensity of which is proportional to the absolute value of the potential energy, and positive electrostatic potentials are shown in blue while green indicates surface areas where the potentials are close to zero. The colour-coded values are then projected onto the 0.002 a.u. isodensity surface to produce a three-dimensional electrostatic potential model. The oxygen atoms with lone pairs have more negative electrostatic potentials (red) whereas the hydrazide hydrogen atoms posses positive electrostatic potentials (blue). Green areas cover parts of the molecule where electrostatic potentials are close to zero (C—C and C—H bonds). Such a representation provides more detailed information regarding electrostatic potential distribution,

---

[1] For interpretation of color in Figs. 9 and 10, the reader is referred to the web version of this article.

Table 6
The Experimental FTIR and FT-Raman frequencies, calculated frequencies, force field along with their relative intensities, probable assignments and potential energy distribution (PED) of 4-hydroxybenzohydrazide.[a]

Experimental wavenumber (cm^{-1})		B3LYP/6-311++G(d,p) calculated wavenumber			B3LYP/6-31G(d,p) calculated wavenumber				B3LYP/aug-cc-pVDZ Calculated wavenumber			Depolarisation ratio	%PED
FTIR	FTR	Unscaled (cm^{-1})	Scaled (cm^{-1})	IR intensity	Unscaled (cm^{-1})	Scaled (cm^{-1})	IR intensity	Raman intensity	Unscaled (cm^{-1})	Scaled (cm^{-1})	IR intensity		
3428 s		3831	3448	76.77	3818	3436	53.79	0.729	3774	3434	65.07	0.28	93νOH
3320 vs	3329vw	3563	3314	6.97	3560	3311	1.42	0.528	3568	3354	1.67	0.70	91ν$_a$NH$_2$
3280 m	3256vw	3520	3274	22.62	3517	3271	10.17	0.832	3486	3277	11.25	0.23	95νNH
3202 m		3470	3227	2.03	3460	3218	4.74	1.000	3420	3215	4.17	0.15	94ν$_s$NH$_2$
		3230	3101	2.45	3254	3091	2.27	0.343	3251	3088	2.73	0.23	92νCH
	3081 w	3204	3076	3.39	3226	3065	3.66	0.506	3221	3060	2.86	0.17	90νCH
		3190	3062	1.86	3210	3050	3.57	0.389	3199	3039	4.50	0.50	94νCH
3012 w		3151	3025	17.66	3165	3007	21.12	0.505	3155	2997	21.20	0.31	90νCH
1622 vs	1623 vs	1720	1634	286.41	1755	1632	222.41	0.254	1740	1618	225.31	0.17	95νC=O
1607 s	1612 s	1689	1638	50.39	1696	1628	27.66	0.112	1674	1624	21.11	0.72	89δNH$_2$
1591 s	1590 s	1647	1598	147.14	1667	1600	141.00	0.501	1663	1613	148.08	0.47	85νCC
1539 m		1622	1573	63.72	1636	1571	53.50	0.074	1631	1582	54.46	0.47	79νCC
1512 s		1541	1495	43.11	1557	1495	32.79	0.053	1543	1497	35.70	0.48	80νCC
1467 m		1473	1429	20.59	1482	1423	15.73	0.143	1473	1429	30.32	0.20	82νCC
1396 m	1397 vw	1460	1416	9.27	1468	1409	26.39	0.051	1458	1414	27.30	0.23	75βNH + 1 9βC=O
1340 w	1342 m	1371	1330	149.64	1390	1334	147.95	0.133	1390	1348	127.06	0.30	81νCC
1329 m	1329 m	1362	1321	177.65	1380	1325	194.75	0.138	1381	1340	209.74	0.32	85νCN
		1332	1292	0.62	1338	1284	5.69	0.004	1320	1280	12.77	0.54	83νCC
1282 m		1311	1272	6.75	1316	1263	48.35	0.049	1315	1276	8.86	0.47	78νCC
1257 vs	1255 vw	1285	1246	116.00	1313	1260	48.62	0.021	1308	1269	68.00	0.10	71βOH + 1 9βC—O
1175 s	1185 vs	1200	1164	6.34	1207	1159	9.84	0.015	1204	1168	1.76	0.29	70νNN + 1 9βN—H
		1194	1158	3.13	1202	1154	24.27	0.024	1197	1161	163.24	0.72	65βCH + 22βC—O
1140 m	1152 s	1185	1149	286.67	1193	1145	267.57	0.120	1180	1145	132.49	0.15	85νCO
1090 w		1129	1095	15.77	1134	1089	13.45	0.005	1118	1084	12.00	0.54	62βCH + 16βCCC
1049 vw	1046 vw	1089	1056	15.32	1096	1052	9.29	0.028	1089	1056	9.73	0.31	60βCH + 20βCCC
995 m		1028	997	1.93	1030	989	1.50	0.003	1023	992	1.64	0.26	59βCCC + 19βC=O
		990	960	1.56	989	949	1.39	0.007	1011	981	0.88	0.61	52βCH + 24βCC
899 m	899 w	952	923	0.73	948	910	0.99	0.010	979	950	4.09	0.71	50γCH + 18γCCC
851 s		897	870	175.30	923	886	160.06	0.024	934	906	133.02	0.63	53ρNH$_2$ + 24βNH
		860	834	28.29	860	826	18.68	0.016	872	846	18.36	0.34	49γCH + 25γCCC
819 vw	824 w	845	820	12.15	851	817	12.32	0.134	849	824	14.07	0.09	48γCH + 22γCCC
	774 vw	813	789	4.66	814	781	5.48	0.023	822	797	4.71	0.74	55γCH + 20γCCC
768 m		775	752	43.33	770	739	50.04	0.006	784	760	32.60	0.75	50βCCC + 21βNH
		710	689	33.08	715	686	43.64	0.014	710	689	32.62	0.47	46βCCC + 29βCH
		692	671	1.92	695	667	1.11	0.017	691	670	0.30	0.19	66βC=O + 19βNH
652 m	659 vw	667	647	18.66	676	649	17.33	0.030	667	647	11.83	0.49	60γNH + 15γC=O
631 s	641 vw	649	630	20.88	652	626	15.55	0.025	646	627	25.10	0.68	52γOH + 22γCO
		588	570	50.91	592	568	42.94	0.022	592	574	41.03	0.46	49βCN + 23βC=O
525 w	525 vw	556	539	16.84	555	533	14.00	0.001	552	535	13.31	0.61	45βCC + 21βNH
487 w	495 vw	508	493	9.32	515	494	4.35	0.002	521	505	6.12	0.73	42βCC + 19βC=O
		422	409	0.89	424	407	0.83	0.002	426	413	2.47	0.56	51γC=O + 17γNH
		414	402	15.71	416	399	16.41	0.001	413	401	16.73	0.33	43γCCC + 22γCO
	359 w	372	361	2.05	379	364	114.40	0.017	396	384	102.00	0.74	42γCCC + 21γCH
	334 w	340	330	107.22	372	357	7.60	0.015	370	359	2.44	0.45	45γCN + 35γC=O
	297 vw	312	303	42.65	320	307	36.72	0.006	321	311	24.00	0.68	46τNH$_2$ + 27γNH
		297	288	14.00	298	286	18.06	0.010	293	284	19.65	0.33	41γCC + 25γNH
	224 vw	235	228	6.96	243	233	10.33	0.004	250	243	15.54	0.67	50βNN(H$_2$) +

(continued on next page)

Table 6 (*continued*)

Experimental wavenumber (cm^{-1})		B3LYP/6-311++G(d,p) calculated wavenumber			B3LYP/6-31G(d,p) calculated wavenumber				B3LYP/aug-cc-pVDZ Calculated wavenumber			Depolarisation ratio	%PED
FTIR	FTR	Unscaled (cm^{-1})	Scaled (cm^{-1})	IR intensity	Unscaled (cm^{-1})	Scaled (cm^{-1})	IR intensity	Raman intensity	Unscaled (cm^{-1})	Scaled (cm^{-1})	IR intensity		
													$19\beta CN$
	164 m	178	173	2.73	183	176	2.93	0.005	187	181	2.50	0.69	$47\gamma NN(H_2)$ + $20\gamma CN$
	126 vs	134	130	5.89	137	132	6.08	0.005	126	122	5.36	0.52	$41\gamma CC + 27\gamma C{=}O$
	110 m	98	95	1.99	102	98	1.68	0.005	103	100	1.44	0.74	$40\gamma CCC + 25\gamma CH$
		46	45	0.90	41	39	1.09	0.021	29	28	1.83	0.74	$39\gamma CCC + 32\gamma CH$

[a] ν – stretching; β – in-plane bending; δ – deformation; ρ – rocking; γ – out of plane bending; ω –wagging and τ – twisting.

by showing the values in a manifold of spatial location around the molecule. The maximum values of positive and negative potential are 0.0835e and −0.1055e, respectively for 4ABH while 0.1149e and −0.1028e for 4HBH.

Natural bond orbital analysis

The atomic charges of 4HBH and 4ABH calculated by NBO analysis using the B3LYP/6-311++G** method is presented in Table 4. The correlation of the atomic charges of 4HBH and 4ABH are illustrated in Fig. 11. In the ring carbon atoms C4 in 4HBH and 4ABH connected to the electronegative O11 and N11, respectively have positive charge while other carbons have negative charges. The greater positive charge of C7 indicates the polar nature of the C═O group. The very high positive charge resides on the hydrazide, hydroxy and amino hydrogen atoms and is due to the difference in electronegativity of these atoms with oxygen and nitrogen atoms, respectively. The significant variation of the charges of C4 atom in these compounds is due to the —OH and —NH_2 substitutions.

Donor–acceptor interactions

Natural bond orbital (NBO) analysis is a useful tool for understanding delocalisation of electron density from occupied Lewis-type (donor) NBOs to properly unoccupied non-Lewis type (acceptor) NBOs within the molecule. The bonding–antibonding interaction can be quantitatively described in terms of the NBO approach that is expressed by means of second-order perturbation interaction energy $E^{(2)}$ [52–54]. This energy represents the estimate of the off-diagonal NBO Fock matrix element. The stabilisation energy $E^{(2)}$ associated with i (donor) → j (acceptor) delocalisation is estimated from the second-order perturbation approach [54] as given below

$$E^{(2)} = q_i \frac{F^2(i,j)}{\varepsilon_j - \varepsilon_i}$$

where q_i is the donor orbital occupancy, ε_i and ε_j are diagonal elements (orbital energies) and $F(i,j)$ is the off-diagonal Fock matrix element.

The second order perturbation analysis of Fock matrix of 4ABH and 4HBH with different types of donor–acceptor interactions and their stabilisation energy are summarised in Table 5. All lone pair–bond pair interactions and only bond pair–bond pair interactions with stabilisation energy greater than 14 kJ mol^{-1} are listed Table 5. In 4ABH molecule, the bond pair donor orbital, $\pi_{CC} \rightarrow \pi^*_{CC}$ interaction between the C3—C4 bond pair and the C1—C2 antibonding orbital gives strongest stabilisation of 25.35 kJ mol^{-1}, C5—C6 bond pair and the C3—C4 antibonding orbital gives strong stabilisation of 23.35 kJ mol^{-1}.

In 4HBH the bond pair donor orbital, $\pi_{CC} \rightarrow \pi^*_{CC}$ interaction between the C3—C4/C5—C6 bond pair and the C1—C2/C3—C4 antibonding orbital gives strongest stabilisation of 24.4 kJ mol^{-1}, C1—C2 bond pair and the C3—C4/C7—O8 antibonding orbital $\pi_{CC} \rightarrow \pi^*_{CC}/\pi^*_{CO}$ interaction gives strong stabilisation of 16.96 and 16.54 kJ mol^{-1}, respectively. From Table 5, it is clear that $n_O(N) \rightarrow \sigma^*_{CO}$ and $n_O(N) \rightarrow \sigma^*_{CC}$ interactions gives more stabilisation than that of the bond pair donor orbital. As well, $\pi_{CC} \rightarrow \pi^*_{CC}/\pi^*_{CO}$ interaction between the ring C—C bond pair and the C—C/C—O antibonding orbital gives more stabilisation energy.

Vibrational assignment and analysis

The FTIR and FT-Raman spectra of the compounds 4ABH and 4HBH are shown in Figs. 12 and 13. The experimental and theoretical frequencies computed by B3LYP method with

Table 7
The Experimental FTIR and FT-Raman frequencies, calculated frequencies, force field along with their relative intensities, probable assignments and potential energy distribution (PED) of 4-aminobenzohydrazide.[a]

Observed wavenumber (cm^{-1})		B3LYP/6-311++G(d,p) Calculated wavenumber			B3LYP/6-31G(d,p) Calculated wavenumber				B3LYP/aug-cc-pVDZ Calculated wavenumber			Depolarisation ratio	%PED
FTIR	FTR	Unscaled (cm^{-1})	Scaled (cm^{-1})	IR intensity	Unscaled (cm^{-1})	Scaled (cm^{-1})	IR intensity	Raman intensity	Unscaled (cm^{-1})	Scaled (cm^{-1})	IR intensity		
3428 s		3682	3424	21.31	3692	3434	14.16	0.314	3676	3419	20.08	0.75	92ν_aNH$_2$
3349 s	3310 w	3593	3341	7.21	3585	3334	1.07	0.469	3577	3327	6.21	0.66	90ν_aNH$_2$
3307 s		3581	3295	38.42	3582	3331	28.75	1.000	3567	3317	35.76	0.18	95νNH
3276 s		3557	3272	25.02	3540	3292	17.62	0.301	3549	3265	24.55	0.14	89ν_sNH$_2$
3235 vs	3234 w	3490	3211	1.67	3473	3230	6.42	0.987	3467	3224	2.10	0.16	94ν_sNH$_2$
		3196	3068	2.61	3217	3088	2.64	0.333	3207	3079	2.55	0.21	96νCH
3058 w	3056 w	3177	3050	11.10	3194	3066	14.40	0.421	3187	3060	10.27	0.17	91νCH
3035 vw		3159	3033	16.39	3176	3049	19.67	0.357	3168	3041	17.68	0.35	95νCH
		3157	3031	14.99	3173	3046	16.50	0.287	3166	3039	13.15	0.54	92νCH
1622 vs		1758	1617	291.42	1795	1616	229.78	0.308	1746	1606	260.36	0.22	97νC=O
		1682	1632	14.80	1688	1620	7.39	0.078	1663	1613	8.19	0.63	90νCC
1605 vs	1599 vs	1664	1614	254.59	1678	1611	283.43	0.581	1658	1608	325.38	0.44	87δNH$_2$
1564 m	1564 m	1647	1598	81.35	1659	1593	9.52	0.136	1638	1589	5.33	0.50	89δNH$_2$
1543 s		1608	1560	6.11	1623	1558	4.89	0.013	1611	1563	6.44	0.27	85νCC
1505 vs	1509 w	1547	1501	23.71	1562	1500	17.18	0.114	1544	1498	21.57	0.42	87νCC
1441 w	1458 vw	1515	1470	132.38	1520	1459	151.54	0.124	1510	1465	137.68	0.33	82βNH
		1462	1418	1.06	1476	1417	0.52	0.002	1459	1415	0.87	0.43	90νCC
	1363 s	1358	1317	1.38	1375	1320	4.08	0.003	1368	1327	3.18	0.42	94νCN
1345 s	1338 m	1332	1292	6.47	1340	1286	11.89	0.009	1325	1285	9.64	0.30	93νCN
1322 vs		1314	1275	6.22	1329	1276	55.24	0.020	1311	1272	1.25	0.11	85νCC
1308 s		1312	1273	57.53	1325	1272	2.22	0.036	1309	1270	71.53	0.65	87νCC
1203 vw		1275	1237	265.42	1286	1235	243.61	0.295	1281	1243	244.88	0.24	83νCC
1192 vw	1195 m	1216	1180	11.16	1224	1175	11.33	0.035	1213	1177	6.96	0.65	75βCH + 12βCCC
1174 vw	1164 w	1192	1156	74.97	1198	1150	57.50	0.112	1187	1151	67.99	0.18	71νNN + 14βN—H
1119 w		1151	1116	11.83	1156	1110	12.29	0.010	1144	1110	11.13	0.57	65βCH + 16βCCC
		1077	1045	0.56	1086	1043	0.32	0.005	1074	1042	0.60	0.75	61βCH + 12βCCC
		1043	1012	37.38	1053	1011	31.20	0.021	1044	1013	37.71	0.54	63βCH + 15βCCC
965 m	971vw	1021	990	15.37	1023	982	9.12	0.002	1014	984	9.65	0.46	59γCH + 12γCCC
956 m		984	954	1.09	981	942	1.15	0.006	985	955	0.87	0.61	51γCH + 16γCCC
941 w		956	927	3.26	954	916	5.70	0.009	954	925	2.50	0.45	56γCH + 19γCCC
884 w	895 m	921	893	32.85	934	897	33.08	0.080	923	895	34.49	0.09	49ρNH$_2$ + 25βCCC
843 s		850	825	38.35	850	816	36.35	0.033	849	824	37.29	0.18	52ρNH$_2$ + 27βNH
		839	814	7.60	845	811	9.93	0.084	840	815	9.69	0.18	41βCCC + 24βCH
777 w	781vw	823	798	3.69	827	794	4.41	0.023	819	794	3.37	0.69	40γCH + 26βCN
		778	755	23.22	790	758	69.63	0.011	781	758	27.19	0.71	45βCCC + 28βCH
715 w		753	730	101.60	766	735	52.12	0.006	763	740	71.98	0.65	41γNH + 17γNN
653 m	650 w	705	684	18.17	702	674	9.03	0.002	704	683	19.39	0.61	52βC=O + 14βNH
639 m		653	633	0.28	654	628	0.38	0.024	648	629	0.18	0.75	46ωNH$_2$ + 26γCCC
620 m		626	607	15.66	630	605	13.35	0.006	624	605	15.69	0.56	47ωNH$_2$ + 24γNH
517 m		531	515	30.42	551	529	79.34	0.024	531	515	18.92	0.63	42βCCC + 21βCH
	495 vw	526	510	59.36	542	520	135.44	0.019	519	503	56.89	0.63	43βCCC + 18βCH
		493	478	281.24	509	489	272.97	0.042	482	468	164.82	0.62	46βCC + 19βC=O
		466	452	83.02	472	453	30.76	0.008	459	445	187.25	0.49	51βCN + 15βNH
		421	408	0.97	422	405	0.83	0.002	421	408	1.42	0.53	49γC=O + 20γNH
	353 vw	386	374	1.75	387	372	2.06	0.001	384	372	2.39	0.75	46γCN + 22γCCC

(*continued on next page*)

Table 7 (*continued*)

Observed wavenumber (cm^{-1})		B3LYP/6-311++G(d,p) Calculated wavenumber			B3LYP/6-31G(d,p) Calculated wavenumber				B3LYP/aug-cc-pVDZ Calculated wavenumber			Depolarisation ratio	%PED
FTIR	FTR	Unscaled (cm^{-1})	Scaled (cm^{-1})	IR intensity	Unscaled (cm^{-1})	Scaled (cm^{-1})	IR intensity	Raman intensity	Unscaled (cm^{-1})	Scaled (cm^{-1})	IR intensity		
	335 vw	338	328	6.25	340	326	5.89	0.015	337	327	7.93	0.35	43βCN(H_2)+17βCCC
		330	320	15.86	334	321	17.23	0.004	335	325	13.33	0.69	41γCN(H_2)+25γNH
	309 vw	315	306	5.94	319	306	5.81	0.014	315	306	5.50	0.51	39τNH_2 + 28γNH
		278	270	1.92	285	274	1.52	0.002	281	273	2.26	0.74	40βNN + 27βNH
	213 vw	186	180	9.24	191	183	13.43	0.001	186	180	11.74	0.67	38γCC + 31γC=OH
		161	156	65.84	159	153	70.18	0.010	146	142	51.38	0.56	42γNN + 29γNH
	116 s	130	126	4.18	134	129	4.17	0.004	132	128	5.13	0.71	39γCCC + 30γCH
		88	85	1.53	93	89	2.15	0.006	89	86	1.98	0.75	43γCCC + 36γCH
		58	56	6.99	64	61	5.62	0.014	57	55	6.79	0.71	37γCCC + 34γCH

[a] ν – stretching; β – in-plane bending; δ – deformation; ρ – rocking; γ – out of plane bending; ω –wagging and τ – twisting.

6-311++G**, 6-31G** and aug-cc-pVDZ basis sets along with their relative intensities, probable assignments and potential energy distribution (PED) of 4ABH and 4HBH are summarised in Tables 6 and 7, respectively.

C—H vibrations

The aromatic C—H stretching vibrations lie in the range 3100—3000 cm^{-1} [55]. The C—H stretching vibrations of 4ABH are seen in IR spectrum at 3058 and 3035 cm^{-1} while in 4HBH the bands are observed at 3081(Raman) and 3012 (IR) cm^{-1}. The potential energy (PED) contribution of the aromatic stretching modes indicates that these are also highly pure modes like the carbon–carbon stretching fundamentals. In accordance with the bending vibrations of benzene [56] the peaks seen at 1090, 1049 cm^{-1} (IR) and 1046 cm^{-1} (Raman) in 4HBH spectra are attributed to the C—H in-plane bending vibrations. The bands observed at 1192, 1119 cm^{-1} (IR) and 1195 cm^{-1} (Raman) in the spectra of 4ABH are assigned to the C—H in-plane bending vibrations. The ring C—H out of plane bending vibrations of 4HBH are seen in the infrared spectrum at 965, 956, 941 and 777 cm^{-1} whereas in 4ABH the same vibrations are seen at 899, 824 and 774 cm^{-1} in Raman spectrum. The PED contributions reveals that the C—H in-plane and out of plane bending vibrations have substantial overlapping with the ring C—C—C in-plane and out of plane bending modes, respectively [57].

Carbon vibrations

The aromatic ring carbon–carbon stretching modes of benzene and its derivatives are noticed in the range 1650–1200 cm^{-1} [56,58]. Strong to medium lines observed in the IR spectrum of 4HBH at 1591, 1539, 1512, 1467, 1340 and 1282 cm^{-1} are ascribed to the C—C stretching modes. The C—C stretching modes of 4ABH are observed as very strong to weak lines in the IR spectrum at 1543, 1505, 1322, 1308 and 1203 cm^{-1}. With reference to vibrational modes of benzene [56] the C—C—C in-plane bending and out of plane bending modes are assigned. The lines identified at 517 (IR) and 495 cm^{-1} (Raman) are assigned to C—C—C in-plane bending vibrations of 4ABH and a strong line identified at 116 cm^{-1} in Raman is assigned to C—C—C out of plane bending vibration. The C—C—C in-plane and out of plane bending modes of 4HBH are seen at 768 cm^{-1} in IR and 359 cm^{-1} in Raman, respectively. In 4HBH spectra C—C in-plane and out of plane bending modes are found at 525, 487 (IR) and 126 (Raman) cm^{-1}.

C=O, C—O and O—H vibrations

The carbonyl C=O stretching modes are reported in the region 1750–1650 cm^{-1} [38]. The carbonyl stretching frequency is observed at 1622 cm^{-1} in IR spectrum of 4HBH and 4ABH. The low frequency of C=O stretching is due to the nitrogen lone pair electron being delocalized towards the carbonyl end and the electron donating nature of the hydroxyl and amino substituents [38]. The C=O in-plane bending mode of 4ABH is assigned to the wavenumber 653 cm^{-1} in the infrared and at 650 cm^{-1} in Raman spectra. In 4HBH, the same has been calculated with B3LYP/6-311++G** method is 671 cm^{-1}. As expected the C—O stretching mode of 4HBH is identified at 1140 cm^{-1} in the IR and at 1152 cm^{-1} in Raman spectra. The stretching frequency of O—H in 4HBH is identified at 3428 cm^{-1} in IR spectrum. The O—H in-plane bending mode of 4HBH is identified at 1257 cm^{-1} in the IR and at 1255 cm^{-1} in Raman spectra whereas the out of plane bending mode is identified at 631 cm^{-1} in the IR and at 641 cm^{-1} in Raman spectra.

Table 8
Frequency correlation of 4-hydroxybenzohydrazide and 4-aminobenzohydrazide with benzohydrazide vibrations.[a]

Molecule	ν_aNH_2		νNH		ν_sNH_2		νC=O		δNH_2		νCN		νNN		γNH	
	A	B	A	B	A	B	A	B	A	B	A	B	A	B	A	B
4HBH	3320 vs	3314	3280 m	3274	3202 m	3227	1622 vs	1634	1607 s	1638	1329 m	1321	1175 vs	1164	652 m	647
4ABH	3349 s	3341	3307 s	3295	3235 vs	3211	1622 vs	1617	1605 vs	1614	1345 s	1292	1174 vw	1156	715 w	730
BH[a]	3300 s	3315	3291 s	3275	3213 s	3230	1661 s	1672	1616 vs	1638	1361 s	1345	1165 m	1169	675 s	650

[a] BH = benzohydrazide [38]; 4HBH = 4-hydroxybenzohydrazide; 4ABH = 4-aminobenzohydrazide; A = Experimental values; B = Theoretical (B3LYP/6-311++G**) values.

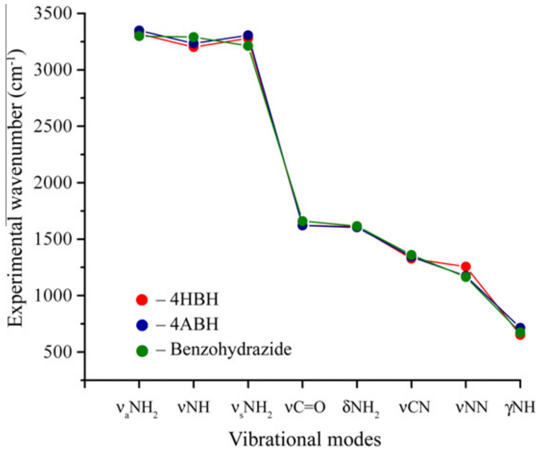

Fig. 14. Correlation of some important fundamental modes of benzohydrazide, 4-aminobenzohydrazide (4ABH) and 4-hydroxybenzohydrazide (4HBH).

—NH and —NH_2 vibrations

The bands of very strong to medium intensity observed at 3320 and 3213 cm^{-1} in the infrared spectrum are assigned to the —NH_2 asymmetric and symmetric stretching modes of 4HBH, respectively. Contrasting, the bands due —NH_2 stretching vibrations in 4ABH exists at higher wavenumbers with deviations in the range 30–100 cm^{-1}. The —NH_2 asymmetric stretching vibration of hydrazide group in 4ABH appears at 3349 cm^{-1} in IR and at 3310 cm^{-1} in Raman spectra while the symmetric stretching is observed at 3235 cm^{-1} in IR and at 3310 cm^{-1} in Raman. The amino group stretching (—NH_2) in 4ABH are dwell in slightly higher wavenumber than that of hydrazide —NH_2 bands. Strong band at 3428 cm^{-1} in IR is due to asymmetric stretching vibration of the amino group while the band at 3276 cm^{-1} in IR is due to symmetric stretching. In 4ABH, —NH_2 deformation mode of hydrazide group is identified at 1605 cm^{-1} in IR and at 1599 cm^{-1} in Raman spectra while a red shift is observed in the deformation mode of amino group and is seen in at 1564 cm^{-1} in IR spectrum. Strong bands in IR at 1607 cm^{-1} and at 1612 cm^{-1} in Raman are assigned to the —NH_2 deformation mode of 4HBH. The N—H stretching vibration of hydrazide group in 4HBH appears at 3280 cm^{-1} in IR and at 3256 cm^{-1} in Raman spectra whereas a blue shift is observed in 4ABH molecule and the corresponding band is found at 3307 cm^{-1}. The other fundamental modes of 4HBH and 4ABH are also assigned in accordance with literature [38] and are presented in Tables 6 and 7.

Frequency correlation

In order to explain the substituents effects on the fundamental frequencies, some important fundamental modes of 4ABH and 4HBH are correlated with the parent benzohydrazide modes and are presented in Table 8. These effects are pictorially illustrated in Fig. 14. The C=O stretching, C—N stretching and —NH_2 deformations of 4ABH and 4HBH are observed in the lower wavenumber region than that of benzohydrazide. This is due to the electron donating nature of —OH and —NH_2 groups which in turn induce the delocalization of the π-electrons towards the C=O group. The asymmetric (3349 cm^{-1}) and symmetric (3235 cm^{-1}) —NH_2 vibrations of 4ABH is observed in the higher wavenumber than in benzohydrazide (3300 and 3213 cm^{-1}). In the case of 4HBH the asymmetric stretching vibration is 20 cm^{-1} more than that of benzohydrazide while the symmetric stretching is 11 cm^{-1} less than in benzohydrazide. The higher —NH_2 stretching wavenumber is due to the electron donating nature of the amino group. A blue shift is observed in the N—H stretching of 4ABH than in benzohydrazide. The substituent effect is negligible on the N—N stretching frequency and is well correlated with the corresponding mode of benzohydrazide.

Conclusion

Experimental and theoretical vibrational spectroscopic studies and DFT calculations of 4-hydroxybenzohydrazide and 4-aminobenzohydrazide using FTIR and FT-Raman spectral data have been presented in this investigation. A comparative study on the equilibrium geometries, structural parameters and harmonic frequencies of title molecules were provided at DFT level of theory utilising 6-31G**, 6-311++G** and aug-cc-pVDZ basis sets. In 4ABH the mean planes of the benzene ring and the planar hydrazide group are inclined at 28.6 with respect to each other. But the mean planes of the benzene ring and the planar hydrazide group of 4HBH are inclined at 24.5 with respect to each other.

The most stable conformer of 4HBH is more stable by 12.47 kcal mol^{-1} than the stable conformer of 4ABH. Except hydrazide hydrogens, the 4ABH and 4HBH molecules are essentially planar as evidenced by the C6—C1—C7—O8, N10—N9—C7—C1 and N10—N9—C7—O8 torsion angles of −22.6°, −178.8° and 1.0° for 4ABH while these are −23.3°, −23.2° and 158.5°, respectively. The heat capacity, entropy and enthalpy change of 4-aminobenzohydrazide (4ABH) is found to be more than in 4-hydroxybenzohydrazide (4HBH) in the range 50–700 °C.

The frontier orbital energy gaps $E_g = E_{LUMO} - E_{HOMO}$ in case of 4HBH and 4ABH is found to be 0.1969 and 0.1875 a.u., respectively. The MEP reveals that the maximum values of positive and negative potentials of 4ABH are 0.0835e and −0.1055e, respectively while 0.1149e and −0.1028e for 4HBH.

The C=O stretching, C—N stretching and —NH_2 deformations of 4ABH and 4HBH are observed in the lower wavenumber region than that of benzohydrazide. This is due to the electron donating nature of —OH and —NH_2 groups which in turn induce the delocalization of the π-electrons towards the C=O group. A blue shift is observed in the N—H stretching of 4ABH than in benzohydrazide. The substituent effect is negligible on the N—N stretching frequency and is well correlated with the corresponding mode of benzohydrazide.

References

[1] M. Ding, Progr. Polym. Sci. 32 (2007) 623–668.
[2] X.Z. Fang, Z.H. Yang, S.B. Zhang, L.X. Gao, M.X. Ding, Polymer 45 (2004) 2539–2549.
[3] M. Hasegawa, N. Sensui, Y. Shindo, R. Yokota, Macromolecules 32 (1999) 387–396.
[4] P.M. Hergenrother, K.A. Watson, J.G. Smith Jr., J.W. Connell, R. Yokota, Polymer 43 (2002) 5077–5093.
[5] P.G. Gervasi, S.D. Petris, D. Lupinacci, Eur. Polym. J. 11 (1975) 233–239.
[6] N.A. Mohamed, Polym. Degrad. Stab. 44 (1994) 33–42.
[7] N.A. Mohamed, A.O. Hamad Al–Dossary, Polym. Degrad. Stab. 79 (2003) 61–75.
[8] C.S. Wang, T.S. Leu, Polymer 41 (2000) 3581–3591.
[9] S. Mehdipour –Ataei, Y. Sarrafi, H. Hatami, Eur. Polym. J. 40 (2004) 2009–2015.
[10] M.S. Butt, Z. Akhter, M. Zafar-Uz-Zaman, A. Munir, Eur. Polym. J. 41 (2005) 1638–1646.
[11] A.H. Frazer, W. Sweeny, F.T. Wallenberger, J. Polym. Sci. A 2 (1964) 1157–1160.
[12] U. Ashiq, R. Ara, M. Mahroof–Tahir, Z.T. Maqsood, K.M. Khan, S.N. Khan, H. Siddiqui, M.I. Choudhary, Chem. Biodivers. 5 (2008) 82–92.
[13] R. Ara, U. Ashiq, M. Mahroof-Tahir, Z.T. Maqsood, K.M. Khan, M.A. Lodhi, M.I. Choudhary, Chem. Biodivers. 4 (2007) 58–71.
[14] Z.T. Maqsood, K.M. Khan, U. Ashiq, R.A. Jamal, Z.H. Chohan, M. Mahroof–Tahir, C.T. Supuran, J. Enz. Inhib. Med. Chem. 21 (2006) 37–42.
[15] K.S. Markley, Fatty Acids, their Chemistry, Properties and Uses, InterScience Publishers, New York, 1964. pp. 1604–1608.
[16] I. Mir, M.T. Siddiqui, A. Comrie, Tetrahedron 26 (1970) 5235–5237.
[17] E. Degener, H. Scheinplug, H.G. Schemelzer, Brit. Patent No.: 1035474, 1967.
[18] R. Cavier, R. Rips, J. Med. Chem. 8 (1965) 706–709.
[19] D.A. Raval, S.D. Toliwal, J. Oil Tech. Assoc. India 26 (1994) 27–29.
[20] E.A. Yousef, M.E. Zaki, M.G. Megahed, Heterocycl. Commun. 9 (2003) 293–298.
[21] D.L. Trepanier, E.R. Wagner, G. Harris, A.D. Rudzik, J. Med. Chem. 9 (1966) 881–885.
[22] K.K. Bedia, O. Elcin, U. Seda, K. Fatma, S. Nathaly, R. Sevim, A. Dimoglo, Eur. J. Med. Chem. 41 (2006) 1253–1261.
[23] H. Yin, J. Cui, Y. Qiao, Polyhedron 27 (2008) 2157–2166.
[24] G.M. Sheldrick, Acta Cryst. A64 (2008) 112–122.
[25] K.K. Vijayaraj, B. Narayana, B.V. Ashalatha, N. Suchetha Kumari, B.K. Sarojini, Eur. J. Med. Chem. 42 (2007) 425–429.
[26] A.H. Abadi, A.A.H. Eissa, G.S. Hassan, Chem. Pharm. Bull. 51 (2003) 838–844.
[27] C.G. Bonde, N.J. Gaikwad, Bioorg. Med. Chem. 12 (2004) 2151–2161.
[28] S.V. Bhandari, A.A. Patil, V. Sarkate, S.G. Gore, K.G. Bothra, Bioorg. Med. Chem. 17 (2009) 390–400.
[29] K. Sugano, H. Hamada, M. Machida, H. Ushio, J. Biomol. Screen 6 (2001) 189–196.
[30] S. Vijayakumar, A. Adhikari, B. Kalluraya, K. Chandrasekharan, Optical Mater. 31 (2009) 1564–1569.
[31] K.V. Sujith, K.B. Manjunatha, B. Kalluraya, G. Umesh, R. Vijayalakshmi, Optics Laser Technol. 42 (2010) 741–748.
[32] R.M. Srivastava, M. Braga, R. Longo, N.S.S. Magalhães, J. Mol. Struct. (1996) 267–272.
[33] L. Wen, H. Yin, W. Li, K. Li, Acta Cryst. E65 (2009) o2623.
[34] C.-G. Fan, M.-Z. Song, Acta Cryst. E65 (2009) o2679.
[35] H.K. Fun, K.V. Sujith, P.S. Patil, B. Kalluraya, S. Chantrapromma, Acta Cryst. E64 (2008) o1961–o1962.
[36] Mohammad Ali Kamyabi, S. Shahabi, H. Hosseini–Monfared, J. Chem. Eng. Data 53 (2008) 2341–2345.
[37] A.K. Singh, S. Kumari, K. Ravi Kumar, B. Sridhar, M. Wrzecion, J. Mroziński, T.R. Rao, Polyhedron 28 (2009) 2599–2604.
[38] V. Arjunan, T. Rani, C.V. Mythili, S. Mohan, Spectrochim. Acta 79A (2011) 486–496.
[39] A. Haider, Z. Akhter, H.M. Siddiqi, E.R.T. Tiekink, J. Chem. Crystallogr. 40 (2010) 397–401.
[40] A.D. Becke, Phys. Rev. A 38 (1988) 3098–3101.
[41] A.D. Becke, J. Chem. Phys. 98 (1993) 5648–5652.
[42] C. Lee, W. Yang, R.G. Parr, Phys. Rev. B 37 (1988) 785–790.
[43] M.J. Frisch, G.W. Trucks, H.B. Schlegel, G.E. Scuseria, M.A. Robb, J.R. Cheeseman, J.A. Montgomery, Jr., T. Vreven, K.N. Kudin, J.C. Burant, J.M. Millam, S.S. Iyengar, J. Tomasi, V. Barone, B. Mennucci, M. Cossi, G. Scalmani, N. Rega, G.A. Petersson, H. Nakatsuji, M. Hada, M. Ehara, K. Toyota, R. Fukuda, J. Hasegawa, M. Ishida, T. Nakajima, Y. Honda, O. Kitao, H. Nakai, M. Klene, X. Li, J.E. Knox, H.P. Hratchian, J.B. Cross, C. Adamo, J. Jaramillo, R. Gomperts, R.E. Stratmann, O. Yazyev, A.J. Austin, R. Cammi, C. Pomelli, J.W. Ochterski, P.Y. Ayala, K. Morokuma, A. Voth, P. Salvador, J.J. Dannenberg, V.G. Zakrzewski, S. Dapprich, A.D. Daniels, M.C. Strain, O. Farkas, D.K. Malick, A.D. Rabuck, K. Raghavachari, J.B. Foresman, J.V. Ortiz, Q. Cui, A.G. Baboul, S. Clifford, J. Cioslowski, B.B. Stefanov, G. Liu, A. Liashenko, P. Piskorz, I. Komaromi, R.L. Martin, D.J. Fox, T. Keith, M.A. Al-Laham, C.Y. Peng, A. Nanayakkara, M. Challacombe, P.M.W. Gill, B. Johnson, W. Chen, M.W. Wong, C. Gonzalez, J.A. Pople, Gaussian Inc., Wallingford, CT, 2004.
[44] H. Fuhrer, V.B. Kartha, K.L. Kidd, P.J. Kruger, H.H. Mantsch, Computer Program for Infrared and Spectrometry, Normal Coordinate Analysis, vol. 5, National Research Council, Ottawa, Canada, 1976.
[45] R.I. Dennington, T. Keith, J. Millam, GaussView, Version 5.0.8, Semichem. Inc. Shawnee Mission, KS, 2008.
[46] V. Krishnakumar, G. Keresztury, T. Sundius, R. Ramasamy, J. Mol. Struct. 702 (2004) 9–21.
[47] M. Sánchez–Lozano, E.M. Vázquez–López, J.M. Hermida–Ramón, C.M. Estévez, Polyhedron 30 (2011) 953–962.
[48] R.A. Jamal, U. Ashiq, M.N. Arshad, Z.T. Maqsood, I.U. Khan, Acta Cryst. E65 (2009) o1764.
[49] J.B. Ott, J. Boerio-Goates, Chemical Thermodynamics: Principles and Applications, vol. I, Academic Press, New York, 2000.
[50] J.M. Seminario, Recent Developments and Applications of Modern Density Functional Theory, vol. 4, Elsevier, 1996. pp. 800–806.
[51] R.H. Petrucci, W.S. Harwood, F.G. Herring, J.D. Madura, General Chemistry: Principles and Modern Applications, ninth ed., Pearson Education Inc., New Jersey, 2007.
[52] A.E. Reed, R.B. Weinstock, F. Weinhold, J. Chem. Phys. 83 (1985) 735–746.
[53] A.E. Reed, F. Weinhold, J. Chem. Phys. 78 (1983) 4066–4073.
[54] J.P. Foster, F. Weinhold, J. Am. Chem. Soc. 102 (1980) 7211–7218.
[55] R.M. Silverstein, G.C. Bassler, T.C. Morrill, Spectrometric Identification of Organic Compounds, fifth ed., JohnWiley & Sons, Inc., New York, 1981.
[56] L.J. Bellamy, The Infrared Spectra of Complex Molecules, third ed., Wiley, New York, 1975.
[57] V. Arjunan, S. Mohan, S. Subramanian, B. Thimme Gowda, Spectrochim. Acta 60A (2004) 1141–1159.
[58] G. Varsanyi, Assignments for Vibrational Spectra of Seven Hundred Benzene Derivatives, vol. I, Adam Hilger, London, 1974.